nature electronics

SUPPLEMENTARY INFORMATION

https://doi.org/10.1038/s41928-018-0190-1

In the format provided by the authors and unedited.

Optimally diverse communication channels in disordered environments with tuned randomness

Philipp del Hougne[1,3]*, Mathias Fink[1] and Geoffroy Lerosey[2]*

[1]Institut Langevin, CNRS UMR 7587, ESPCI Paris, PSL Research University, Paris, France. [2]Greenerwave, ESPCI Paris Incubator PC'up, Paris, France. [3]Present address: Institut de Physique de Nice, CNRS UMR 7010, Université Côte d'Azur, Nice, France. *e-mail: philipp.delhougne@gmail.com; geoffroy.lerosey@greenerwave.com

Supplementary Discussion

I. Independence of Different Experimental Realizations

We state in the main text that we repeat the experiment for different orientations of the mode-stirrer shown in Figure 1 of the main text and that this constitutes independent realizations with a completely different random cavity geometry. In this section, we provide details of our experimental characterization of the mode-stirrer. We show that the mode-stirrer must be rotated by at least $\Delta\theta_{dc} = 12°$ to access a new, independent realization.

To determine $\Delta\theta_{dc}$, we measure the transmission $S(f, \theta)$ between two antennas placed inside the cavity for 360 positions of the mode-stirrer, covering the interval $0° \leq \theta \leq 360°$ in steps of $1°$. The frequency is swept across the frequency range $1.8175\ \text{GHz} < f < 3.1225\ \text{GHz}$. We then compute the correlation $\mathcal{C}(\theta, \theta')$ between two mode-stirrer orientations θ and θ' as

$$\mathcal{C}(\theta, \theta') = \frac{\left|\langle S(\theta) S^*(\theta')\rangle_f\right|}{\sqrt{\langle |S(\theta\ )|^2\rangle_f}\sqrt{\langle |S(\theta')|^2\rangle_f}},$$

where $\langle \cdots \rangle_f$ denotes the average of the enclosed quantity over the measured frequency interval. The obtained matrix $\mathcal{C}(\theta, \theta')$ is shown in Supplementary Figure 1a. It is symmetric and has a unit diagonal (by definition). Aligning this matrix and averaging over one dimension yields Supplementary Figure 1b from which we can deduce $\Delta\theta_{dc} = 12°$.

II. Pathloss

In this section, we substantiate our observation stated in the main text that pathloss remains unaltered (on average) by our procedure of optimizing the channel diversity. This observation is also an important justification for the subsequent sections where we show algebraically that under the assumption of fixed pathloss a flat distribution of singular values maximizes channel diversity and channel capacity.

The pathloss ξ of an $n \times n$ channel matrix is defined as

$$\xi = \frac{1}{n^2} \sum_{\alpha=1}^{n} \sum_{\beta=1}^{n} \left| H_{\alpha,\beta} \right|^2 .$$

For the 30 realizations of the experiment that we performed for channel matrices of different sizes ($2 \leq n \leq 7$), we display in Supplementary Figure 2 histograms of the pathloss before and after optimizing the channel diversity, as well as of the change in pathloss. Supplementary Figure 3 summarizes the average values of these quantities, as well as the respective standard deviations.

Note that the subsequent pathloss results are given in **arbitrary units** (a.u.), since we did not perform a calibration step to account for losses in the coaxial cables (about 3 m between VNA and antennas) and the insertion losses of the RF switches. (The antenna coupling was not an important source of losses because we used monopole antennas resonant at the operating frequency.) For the results presented in the main text based on monochromatic transmission measurements, a calibration was not necessary: multiplying the channel matrix by a non-zero complex-valued number does not alter its effective rank. Moreover, proper calibration of a setup including RF switches is challenging. For our purposes, it was not necessary.

Averaged over all realizations and different sizes of the channel matrix, we find

$$\xi_{\mathrm{INIT}} = (24.1 \pm 7.3) \times 10^{-5}\ \mathrm{a.u.}$$

$$\xi_{\mathrm{FIN}} = (22.7 \pm 6.7) \times 10^{-5}\ \mathrm{a.u.}$$

$$\Delta\xi = \xi_{\mathrm{INIT}} - \xi_{\mathrm{FIN}} = (1.5 \pm 6.0) \times 10^{-5}\ \mathrm{a.u.}$$

The stated uncertainties indicate the standard deviation.

We thus conclude that given our experimental data, there is no statistically significant change in pathloss as we optimize the channel diversity. Note that due to the logarithmic scaling in the generalized version of Shannon's Law, small changes in SNR or pathloss would have very little impact in any case.

III. Is it Always Advantageous to Operate with Maximal Channel Diversity?

In this section, we discuss if it is always (for all possible SNR values) *advantageous* in terms of capacity to operate with maximal channel diversity. In other words, if the singular value distribution of the channel matrix is the only free parameter (i.e. fixed SNR, fixed pathloss), is a flat distribution always the best choice? First, we get some initial insights by considering the two extremes of perfectly identical and perfectly orthogonal channels; then, we provide a formal algebraic proof to show that the answer to the question is 'yes'.

If channel diversity is the only free parameter, then we assume constant SNR ρ and constant pathloss (i.e. $\sum_{i=1}^{n}\sigma_i^2 = P$, where P is some positive, real-valued constant). We demonstrated in Section II. that this assumption is indeed valid, i.e. that altering the channel diversity does not impact the overall pathloss. In other words, the question corresponds to our experiments in which we alter solely the channel diversity. The two extremes of using perfectly identical or perfectly orthogonal channels correspond to $\sigma_1^2 = P$ and $\sigma_{i\neq 1}^2 = 0$, or $\sigma_i^2 = P/n$, respectively. Equation 1 from the main text then yields $C_{IDENT} = \log_2[1+\rho P/n]$ and $C_{ORTH} = n\log_2[1+\rho P/n^2]$. Then, $C_{ORTH} > C_{IDENT}$ for all positive ρ since $\frac{\partial}{\partial\rho}(C_{ORTH} - C_{IDENT}) = \frac{(n-1)\rho P^2}{\log(2)(n+\rho P)(n^2+\rho P)} > 0$. In Supplementary Figure 4 we plot the dependence of C_{IDENT} and C_{ORTH} on ρ (note in the figure the SNR is given in dB hence the value can become negative, but on a linear scale it is always positive).

To prove more rigorously that a flat singular value spectrum is optimal if channel diversity is the only tunable parameter, first, we recall Eq. 1 of the main text in terms of the square singular values of the channel matrix:

$$C = \sum_{i=1}^{n}\log_2\left(1+\frac{\rho}{n}s_i\right),$$

where $s_i = \sigma_i^2$ is the square of the ith singular value σ_i of **H**.

We wish to maximize $C(s_1, s_2, \cdots, s_n)$ subject to the constraint $\sum_{i=1}^{n} s_i = P$, where P is some positive, real-valued constant. Now, we apply the method of Lagrange multipliers. The Lagrangian for the problem at hand is

$$\mathcal{L}(s_1, s_2, \cdots, s_n, \zeta) = C(s_1, s_2, \cdots, s_n) + \zeta\, g(s_1, s_2, \cdots, s_n),$$

with $g(s_1, s_2, \cdots, s_n) = (\sum_{i=1}^{n} s_i) - P$. The gradients can thus be evaluated as

$$\frac{\partial \mathcal{L}}{\partial s_i} = \frac{\partial}{\partial s_i}\left(\log_2\left(1+\frac{\rho}{n}s_i\right)+\zeta s_i\right) = \frac{\rho}{s_i\rho\ln(2)+n\ln(2)}+\zeta$$

and

$$\frac{\partial \mathcal{L}}{\partial \zeta} = \left(\sum\nolimits_{i=1}^{n} s_i\right) - P$$

yielding

$$\frac{\rho}{s_i\rho\ln(2)+n\ln(2)}+\zeta = 0$$

and

$$\left(\sum\nolimits_{i=1}^{n} s_i\right) - P = 0\,,$$

the latter being the original constraint.

By considering the constraints for s_i and s_j, for $1 \le i \le n$, $1 \le j \le n$ and $i \ne j$,

$$\frac{\rho}{s_i\rho\ln(2)+n\ln(2)}+\zeta = \frac{\rho}{s_j\rho\ln(2)+n\ln(2)}+\zeta$$

which simplifies to

$$s_i = s_j\,.$$

Hence, to maximize $C(s_1, s_2, \cdots, s_n)$ subject to the constraint $\sum_{i=1}^{n} s_i = P$, all s_i have to be identical, quod erat demonstrandum. It is thus always advantageous in terms of the system's capacity to operate at maximum channel diversity if all other parameters remain unchanged. Stated more intuitively, the more effectively independent channels there are, the more information can be transferred.

For completeness, we go on to prove that our optimization functional, the effective rank, is also maximized if the singular values of the channel matrix are all equal, again assuming fixed pathloss. We proceed as before by using the method of Lagrange multipliers. Here, we wish to maximize

$$R_{\text{eff}}(\sigma_1', \sigma_2', \cdots, \sigma_n') = \exp\left(-\sum_{i=1}^{n}\sigma_i'\ln(\sigma_i')\right) = \prod_{i=1}^{n} e^{-\sigma_i'\ln(\sigma_i')},$$

where $\sigma_i' = \sigma_i/(\sum_{i=1}^{n}\sigma_i)$ are the normalized singular values of the channel matrix (see Eq. 2 in the main text), subject to the constraint $\sum_{i=1}^{n}\sigma_i' = 1$. The Lagrangian for the problem at hand is

$$\mathcal{L}(\sigma_1', \sigma_2', \cdots, \sigma_n', \zeta) = R_{\text{eff}}(\sigma_1', \sigma_2', \cdots, \sigma_n') + \zeta\, g(\sigma_1', \sigma_2', \cdots, \sigma_n')\,,$$

with $g(\sigma_1{}', \sigma_2{}', \cdots, \sigma_n{}') = (\sum_{i=1}^{n} \sigma_i{}') - 1$. The gradients can thus be evaluated as

$$\frac{\partial \mathcal{L}}{\partial \sigma_i'} = -\sigma_i'^{-\sigma_i'}(\ln(\sigma_i') + 1)\left(\prod_{j=1, j\neq i}^{n} e^{-\sigma_j' \ln(\sigma_j')}\right) + \zeta$$

and

$$\frac{\partial \mathcal{L}}{\partial \zeta} = \left(\sum\nolimits_{i=1}^{n} \sigma_i{}'\right) - 1\,.$$

This yields

$$0 = -\sigma_i'^{-\sigma_i'}(\ln(\sigma_i') + 1)\left(\prod_{j=1, j\neq i}^{n} e^{-\sigma_j' \ln(\sigma_j')}\right) + \zeta$$

and

$$0 = \left(\sum\nolimits_{i=1}^{n} \sigma_i{}'\right) - 1\,.$$

The latter is once again the original constraint. From the former, it follows for $1 \leq i \leq n$, $1 \leq k \leq n$ and $i \neq k$, that

$$-\sigma_i'^{-\sigma_i'}(\ln(\sigma_i') + 1)\left(\prod_{j=1, j\neq i}^{n} e^{-\sigma_j' \ln(\sigma_j')}\right) + \zeta = -\sigma_k'^{-\sigma_k'}(\ln(\sigma_k') + 1)\left(\prod_{j=1, j\neq k}^{n} e^{-\sigma_j' \ln(\sigma_j')}\right) + \zeta$$

which simplifies to

$$\sigma_i'^{-\sigma_i'}(\ln(\sigma_i') + 1)e^{-\sigma_k' \ln(\sigma_k')} = \sigma_k'^{-\sigma_k'}(\ln(\sigma_k') + 1)e^{-\sigma_i' \ln(\sigma_i')}$$

and then to

$$\frac{\ln(\sigma_i') + 1}{\sigma_i'^{\sigma_i'}} e^{\sigma_i' \ln(\sigma_i')} = \frac{\ln(\sigma_k') + 1}{\sigma_k'^{\sigma_k'}} e^{\sigma_k' \ln(\sigma_k')}$$

which ultimately may be recast as

$$\ln(\sigma_i') = \ln(\sigma_k')\,.$$

This implies $\sigma_i' = \sigma_k'$. Hence, to maximize the effective rank subject to the constraint $\sum_{i=1}^{n} \sigma_i{}' = 1$, all normalized singular values σ_i' have to be identical, quod erat demonstrandum.

IV. Toy Model

Each entry $H_{\alpha,\beta}$ of the channel matrix is an independent transmission measurement in the cavity. Each transmission measurement $S(r_i, r_j, f_0)$, may be interpreted as the Green's function at the working frequency f_0 between the two corresponding antenna positions r_i and r_j, $r_i \neq r_j$. The Green's function may then be decomposed into the contributions from different cavity modes that overlap at the working frequency due to their finite line-widths. Neglecting for clarity's sake the vectorial nature of the electromagnetic field as well as details of the antenna coupling, we can write[1,2]

$$S(r_i, r_j, f_0) \propto \sum_{k=1}^{N} \frac{\Psi_k(r_i)\Psi_k(r_j)}{\frac{4\pi^2}{c^2}(f_0^2 - f_k^2) + 2\pi i f_0 \Gamma_k},$$

where Ψ_k and f_k are the eigenvector and eigenvalue of the *k*th cavity mode that contributes at the working frequency f_0. Γ_k is the line-width of the kth mode. The number of contributing modes N can be estimated with Weyl's law[3,4]. Accounting for the three-dimensional and vectorial nature of our system, this yields

$$N \sim \frac{8\pi f_0^2 V}{c^3} \times \bar{\Gamma},$$

where c is the speed of light, V is the cavity's volume and $\bar{\Gamma}$ is the average modal line-width. In lossy cavities, all modal line-widths are essentially equal to $\bar{\Gamma}$. For our system, the approximation is reasonable to get an idea of the magnitude of N.

For our metallic disordered cavity, we obtain an estimate of the average modal line-width via the decay rate of the inverse Fourier transform of several experimentally measured transmission spectra: $\bar{\Gamma} \sim 4.1$ MHz. We further know that $f_0 = 2.47$ GHz and $V = 1.1$ m^3. Inserting these values into $N \sim \frac{8\pi f_0^2 V}{c^3} \times \bar{\Gamma}$, we find $N \sim 25$.

In a chaotic cavity, Ψ_k are seemingly random[5,6]. We can thus interpret $S(r_i, r_j, f_0)$ as a random walk of N steps in the complex plane.

Using our tunable metasurface we can *effectively* control p modal contributions to $S(r_i, r_j, f_0)$. Note the importance of the term "effectively" here, since one pixel affects of course all modes to some extent. This is a simplification to draft a toy model. p is proportional to the number of metasurface pixels; in previous work[7] (considering the enhancement of the transmitted

intensity between two antennas) we found p to be roughly a third of the number of metasurface pixels.

Now, let us consider the task of achieving optimal channel diversity. We can consider the rows of the channel matrix **H** as n points in an n-dimensional space. The effective rank of **H** is maximal if all n points have the same distance from the origin and if the vectors from the origin to these points are orthogonal to each other.

Clearly, controlling the N modal contributions of each of the n^2 channel matrix entries is illusive. We manage to impose approximately perfect orthogonality up to $n = 4$ where $n^2N = 400$ but we only have 65 metasurface pixels. We also found that approximately perfect orthogonality can be achieved for $n = 2$ where $n^2N = 100$ with roughly 32 pixels – see Supplementary Figure 5a. Moreover, each pixel probably controls even less than one modal contribution on average (see above). To achieve optimal channel diversity, the necessary control is thus far less than the ability to control all modal contributions.

To draft a rough toy model that coveys a sense of how many pixels one may need for a given number of channels, let us consider the n points in n-space that represent the n rows of the channel matrix. Their distance from the origin is on average the same (the result of a series of random walks along each of the n dimensions), so we neglect the need to ensure those distances are equal in the following. If we assume the vector from the origin to the first point (corresponding to the first row of **H**) is fixed somewhere in n-space, ensuring that the vector from the origin to the second point (corresponding to the second row of **H**) is perpendicular to the first one is relatively easy: there are still $n - 1$ dimensions left. It thus takes very little control to ensure the first two rows are orthogonal. Next, assuming the first and second row are now fixed, we must control the third row so that it is perpendicular to the first and second one. Again, since there are $n - 2$ dimensions left, this is an only slightly more challenging task. A possibly somewhat rough approximation is thus to consider the main (dominating) challenge to be the control of the nth row, since it has to be aligned along the only dimension that is still left. The nth row consists of n entries, that is of n independent transmission measurements. Then, the difficulty scales linearly with n.

While we have made several crude approximations in the above,

(i) this toy model roughly explains our observation of a linear scaling of the minimum number of necessary metasurface pixels with the channel matrix size n: it takes 32 pixels to reach perfect channel diversity for $n = 2$, and 65 pixels for $n = 4$;

(ii) the order of magnitude of the required number of pixels agrees with the order of magnitude estimated for N;

(iii) the model conveys to first approximation why the task of achieving optimal channel diversity takes as little control as reported in our work, in comparison to the total number of modal contributions to all n^2 transmission measurements of which the channel matrix consists.

A more rigorous statistical description of our approach would probably require numerical tools found within the realm of random matrix theory to model wave-chaotic systems[5,6]. However, these would have to be adapted to account for tunable boundary conditions before applying them to our problem – hence this is clearly outside the scope of our experimental work reported here.

In Supplementary Figure 5 we present preliminary results of experiments in which we repeated the same procedure of optimizing the channel diversity as in the main text in the metallic cavity, with varying numbers of controllable phase-binary metasurface pixels, for channel matrices of sizes $n = 2$ and $n = 5$. Only 32 phase-binary metasurface pixels are needed to reach optimal channel diversity of a 2×2 channel matrix in our metallic cavity.

V. Improving the Metasurface Design

The employed metasurface is the prototype presented in ref.[8] whose pixels offer phase-binary control over one polarization of the electromagnetic field. There are various opportunities to increase the control of a metasurface pixel over the wave field.

1. Reduce absorption.

   In its current design, the metasurface pixel absorbs about half of the incident energy (see Figure 4a in ref.[8]). By reducing this absorption, more weight can be given to the shaped reflected rays that interacted with the metasurface relative to rays that were reflected by ordinary walls. Recent prototyping suggests that improving details of the metasurface design can reduce absorption at least by a factor of about four.

2. Control both polarizations.

   The current metasurface design only acts on one of two independent polarizations. The concept underlying the metasurface design can be extended to achieve independent control over both polarizations on the same pixel (with two independent bias voltages). Since a chaotic cavity completely mixes all polarizations, this would double the control over the wave field for a fixed metasurface size.
   Recent prototyping suggests that this is indeed feasible, and first experimental results confirm the ability to double the control over the wave field by controlling independently both polarizations (page 35 in ref.[9]).

3. Implement phase-linear control.

   The current metasurface design only offers phase-binary control over the wave field with each pixel. The PIN-diode could be replaced by a variable capacity, enabling the implementation of a phase-linear instead of only phase-binary control.
   The benefit of increasing the available number z of discretized phase values diminishes rapidly. A simple benchmark model that was studied for wave front shaping in optics (focusing a wave on a chosen point behind a multiply scattering layer by shaping the wave

front with z possible phase steps) shows that phase-binary control achieves 40% of the optimum with phase-linear control; $z = 4$ already reaches 80% of the optimum (page 73 in ref.[10]). These results indicate that implementing full phase-linear control is probably not worth the additional cost. However, increasing z from 2 to 4 might be worthwhile.

The above discussion provides indications on how the employed metasurface design could be improved. The decision whether it is more convenient to pursue any or several of these routes in contrast to simply using a larger metasurface could ultimately be driven by economic aspects. Finally, note that our proposed scheme of tweaking a propagation medium's disorder does not rely on the specific design of our metasurface. Although we consider it advantageous, in principle other implementations of tunable impedance surfaces such as mushroom structures could be employed, too.[11,12]

Finally, we point out that the entire optimization procedure could be performed in real time with optimized electronics (e.g. using field-programmable-gate-arrays (FPGAs) instead of the Arduino microcontroller) such that the reflect-array's PIN diodes could be switched at MHz rates. Hardware solutions in that spirit have been reported, for instance, in refs.[13,14], proving that this is technologically possible with the current state-of-the-art.

1 Kuhl, U., Stöckmann, H. & Weaver, R. Classical wave experiments on chaotic scattering. *J. Phys. A* **38**, 10433 (2005).

2 Hemmady, S., Zheng, X., Antonsen Jr, T. M., Ott, E. & Anlage, S. M. Universal statistics of the scattering coefficient of chaotic microwave cavities. *Phys. Rev. E* **71**, 056215 (2005).

3 Weyl, H. Über die asymptotische Verteilung der Eigenwerte. *Nachrichten von der Gesellschaft der Wissenschaften zu Göttingen, Mathematisch-Physikalische Klasse* **1911**, 110-117 (1911).

4 Arendt, W., Nittka, R., Peter, W. & Steiner, F. Weyl's law: Spectral properties of the Laplacian in mathematics and physics. *Mathematical Analysis of Evolution, Information, and Complexity*, 1-71 (2009).

5 Kuhl, U., Legrand, O. & Mortessagne, F. Microwave experiments using open chaotic cavities in the realm of the effective Hamiltonian formalism. *Fortschr. Phys.* **61**, 404-419 (2013).

6 Gradoni, G. *et al.* Predicting the statistics of wave transport through chaotic cavities by the random coupling model: A review and recent progress. *Wave Motion* **51**, 606-621 (2014).

7 Dupré, M., del Hougne, P., Fink, M., Lemoult, F. & Lerosey, G. Wave-Field Shaping in Cavities: Waves Trapped in a Box with Controllable Boundaries. *Phys. Rev. Lett.* **115**, 017701 (2015).

8 Kaina, N., Dupré, M., Fink, M. & Lerosey, G. Hybridized resonances to design tunable binary phase metasurface unit cells. *Opt. Express* **22**, 18881-18888 (2014).

9 del Hougne, P. *Shaping Green's Functions in Cavities with Tunable Boundary Conditions: From Fundamental Science to Applications* PhD thesis, Université Sorbonne Paris Cité, (2018).

10 Popoff, S. *Contrôle spatio-temporel de la lumière en milieux complexes* PhD thesis, Université Paris 7 - Denis Diderot, (2011).

11 Sievenpiper, D. F., Schaffner, J. H., Song, H. J., Loo, R. Y. & Tangonan, G. Two-dimensional beam steering using an electrically tunable impedance surface. *IEEE Trans. Antennas Propag.* **51**, 2713-2722 (2003).

12 Sleasman, T., Imani, M. F., Gollub, J. N. & Smith, D. R. Microwave imaging using a disordered cavity with a dynamically tunable impedance surface. *Phys. Rev. Appl.* **6**, 054019 (2016).

13 Yang, H. *et al.* A programmable metasurface with dynamic polarization, scattering and focusing control. *Sci. Rep.* **6**, 35692 (2016).

14 Gollub, J. *et al.* Large Metasurface Aperture for Millimeter Wave Computational Imaging at the Human-Scale. *Sci. Rep.* **7**, 42650 (2017).

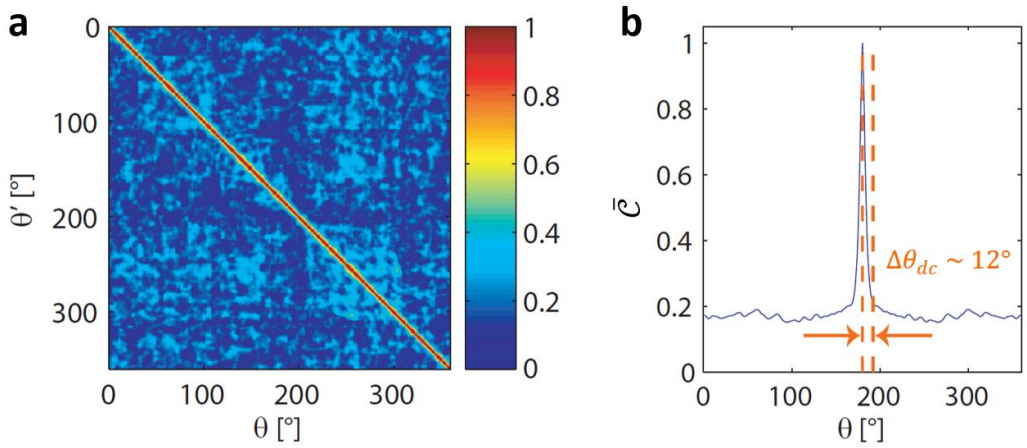

Supplementary Figure 1 | Minimum rotation of the mode-stirrer to access an uncorrelated realization. a, The matrix shows the correlation $\mathcal{C}(\theta, \theta')$ between the spectra corresponding to mode-stirrer orientations θ and θ'. **b,** Aligning this matrix and averaging over one dimension yields $\bar{\mathcal{C}}(\theta)$ from which the result $\Delta\theta_{dc} = 12°$ is extracted.

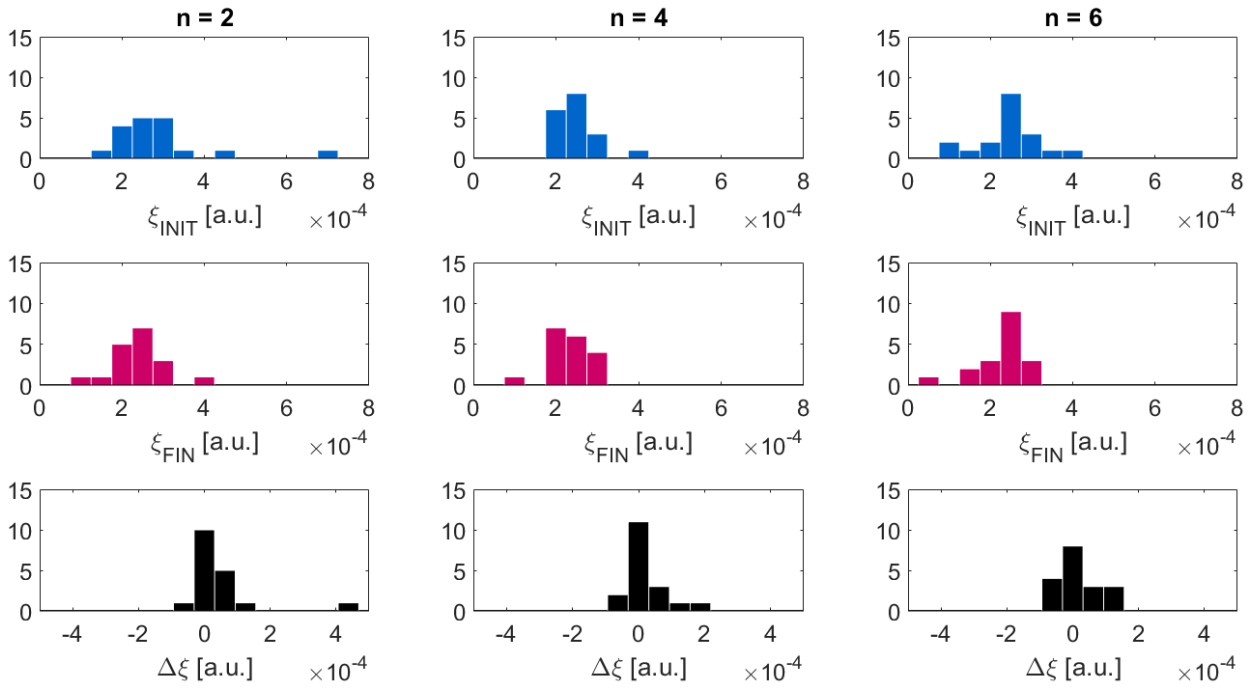

Supplementary Figure 2 | Histograms of experimentally measured pathloss ξ before (blue) and after (red) optimizing the channel diversity. Note that the units of pathloss in this figure are arbitrary (see discussion in Section II.). The figure is based on the same data of 30 realizations as Figure 3 in the main text. The histograms are shown for different sizes of the channel matrix ($n = 2, 4, 6$). Histograms of the difference between initial and final pathloss for each realization are shown in black.

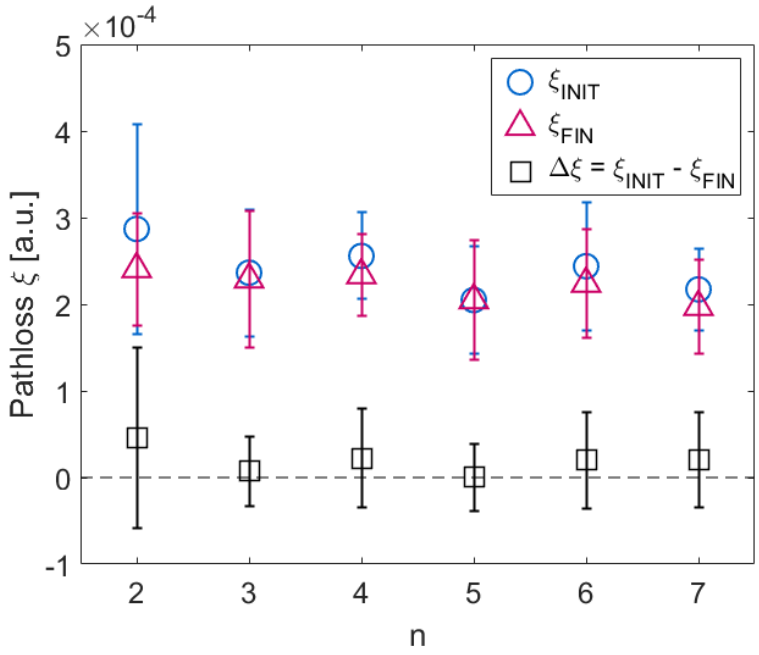

Supplementary Figure 3 | Average value and standard deviation of pathloss before (blue circle) and after (red triangle) optimizing the channel diversity, and the difference (black square). Each data point is based on 30 realizations of the experiment for channel matrices of different sizes n; error bars indicate the standard deviation. Note that pathloss is given in arbitrary units here.

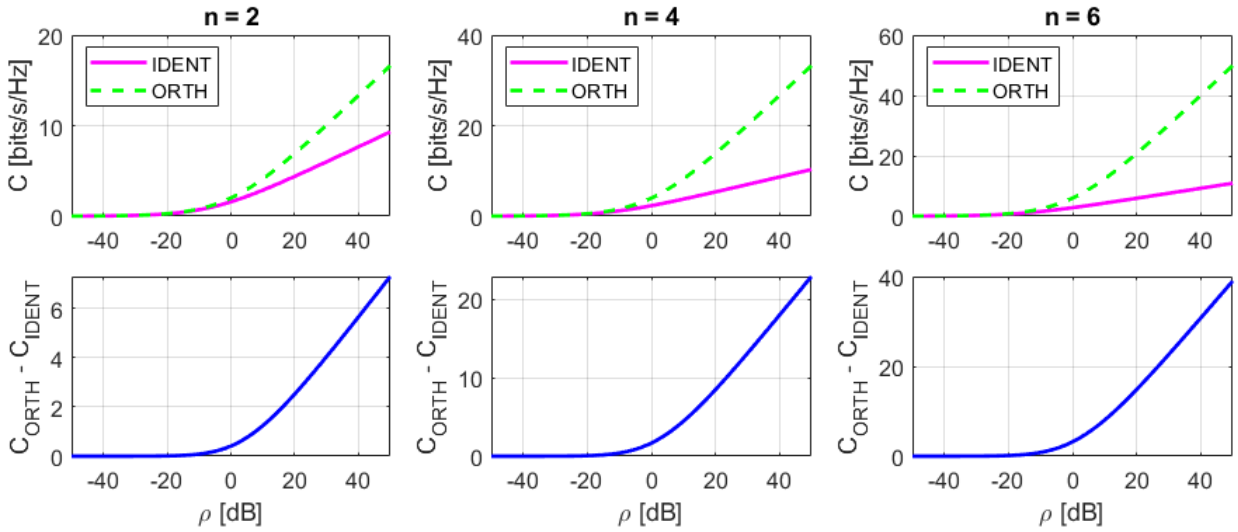

Supplementary Figure 4 | Contrasting the capacity dependence on SNR for the case of perfectly identical or perfectly orthogonal channels, with identical pathloss. See Section III. for further details. The figure was plotted for $P = 1$, different values of P would essentially just shift the curves along the horizontal axis since they can be interpreted as an effectively altered SNR. The figure illustrates that maximum channel diversity is always the best choice.

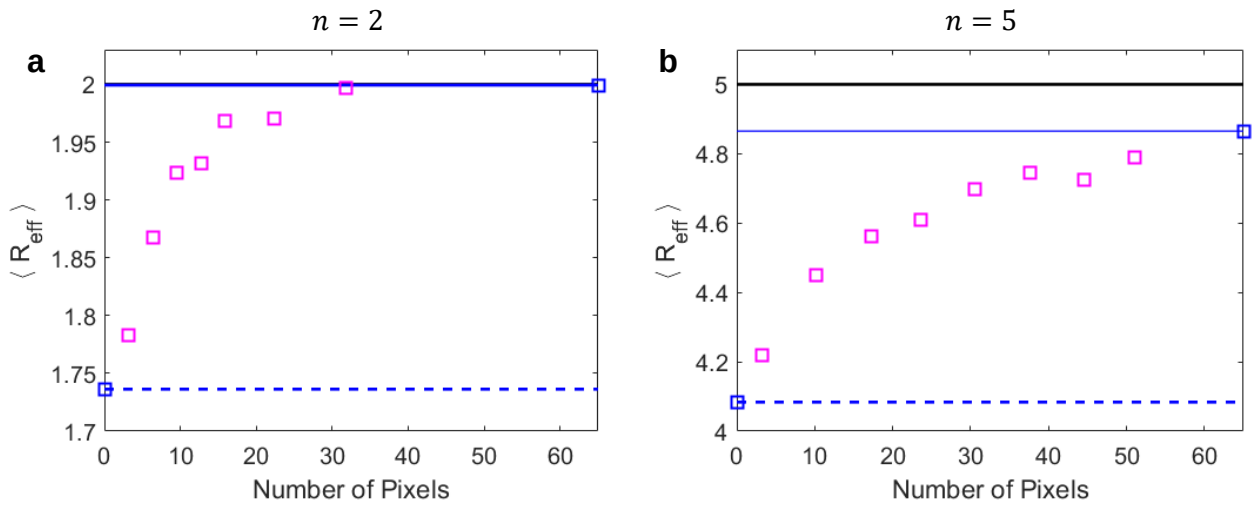

Supplementary Figure 5 | Achieved channel diversity as a function of the number of available phase-binary metasurface pixels. The presented results are averaged over realizations of disorder and displayed for $n = 2$ (**a**) and $n = 5$ (**b**). For reference, the benchmark results from the main text using zero or all 65 pixels are indicated in blue, as well as the orthogonality benchmark in black.

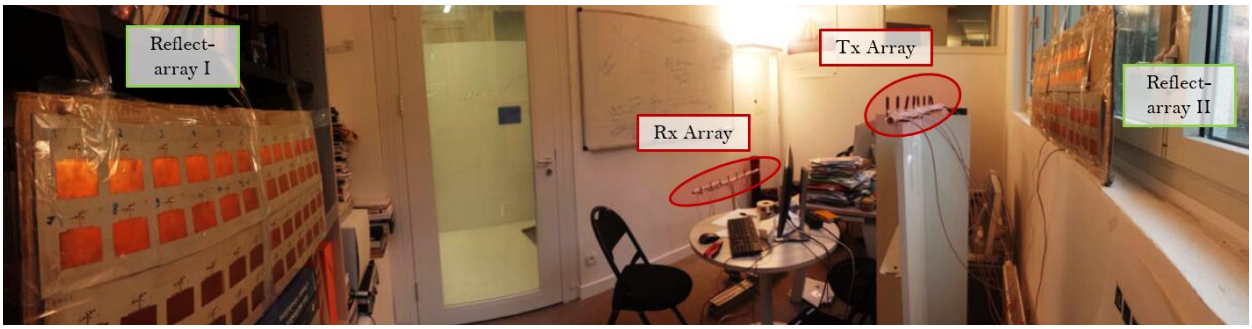

Supplementary Figure 6 | Photographic image of the office room setup. Two antenna arrays are placed in a heavily furnished office of irregular geometry. The two parts of the metasurface reflect-array are also identified in the image.

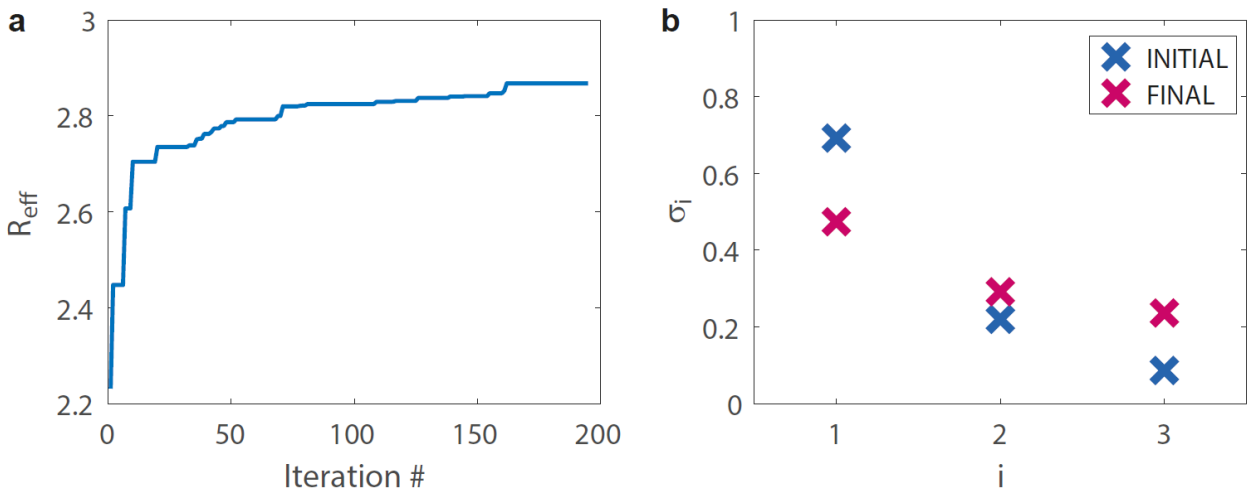

Supplementary Figure 7 | Further details on the realization of the experiment in the office room. Figure 4 of the main text is based on this experiment. The office room is shown in Supplementary Figure 6. **a,** Optimization dynamics as function of the iteration. **b,** Singular value spectrum of the channel matrix before and after optimization in the office room.